[14] R. De Smedt, "Dielectric resonator inside a circular waveguide," *Arch. Elek. Ubertragung (AEU)*, vol. 38, pp. 113–120, Mar. 1984.
[15] R. De Smedt, "Correction factors due to a finite permittivity for a dielectric ring resonator in free space," University of Ghent, Laboratorium voor Elektromagnetisme en Acustica, Internal Report 83-3, May 1983.
[16] P. M. Morse and H. Feshbach, *Methods of Theoretical Physics*, Part II. New York: McGraw-Hill, 1953, pp. 1001–1038.
[17] R. De Smedt, "Boundary conditions of an open infinite region for the finite element method," in *Proc. 3rd. Int. Conf. on Antennas and Propagation, ICAP-83* (Norwich, England), Apr. 1983, pp. 262–266.
[18] M. Gastine, L. Courtois, and J. L. Dormann, "Electromagnetic resonances of free dielectric spheres," *IEEE Trans. Microwave Theory Tech.*, vol. MTT-15, pp. 694–700, Dec. 1967.
[19] R. De Smedt, "Correction due to finite permittivity for a dielectric resonator," in *Proc. 13th Eur. Microwave Conference* (Nürnberg, West Germany), Sept. 1983, pp. 797–802.
[20] J. Van Bladel, *Electromagnetic Fields*. New York: McGraw-Hill, 1964, pp. 211–219.

Ronald De Smedt was born in Ostend, Belgium, on August 18, 1955. He received the degree of electrical engineering from the University of Ghent, Belgium, in 1978.

Since 1978, he has been a Research Assistant at the Laboratory of Electromagnetism and Acoustics, University of Ghent, preparing a Ph.D. dissertation in the area of numerical techniques applied to electromagnetism. His main interest is with small apertures and dielectric resonators.

Theory and Numerical Simulation of a TE_{111} Gyroresonant Accelerator

WILLIAM H. MINER, JR., PETER VITELLO, AND ADAM T. DROBOT

Abstract—**The production of spiral relativistic electron beams in a TE_{111} gyroresonant accelerator cavity for injection into a compact high-harmonic gyrotron is studied. Parametric studies are performed to determine the effects of variations in the background magnetic field amplitude, the RF amplitude in the cavity, and the initial beam voltage on the output beam. The effects of velocity spread and a finite radial extent of the input beam are also discussed. Power curves for obtaining optimum operating regimes for the TE_{111} accelerator are provided.**

I. Introduction

GYROTRONS have successfully generated electromagnetic radiation in the millimeter and submillimeter wavelength ranges via the electron-cyclotron maser instability [1]–[3]. Electromagnetic radiation is produced through the interaction of a relativistic electron beam gyrating about an external magnetic field and an excited cavity mode which grows at the expense of the rotational energy of the beam. The production of relativistic electron beams, with most of its kinetic energy in the form of rotational energy, therefore, plays a crucial role in the development of gyrotron devices.

In this paper, we discuss an "injection system" capable of producing such a beam for use in a compact high-harmonic gyrotron [4], [5]. This system, which consists of a conventional electron gun and a resonant "accelerator" cavity, has two advantages over other systems currently in use: 1) the system is technically simple, and 2) it operates at a relatively low voltage. It also differs from relativistic electron-beam sources used in conventional gyrotrons in that it produces a beam whose Larmor orbits encircle the cavity axis. Conventional gyrotrons operate at the first or second harmonic with a relatively high magnetic field, and with Larmor orbits of the beam particles which are much smaller than the cavity radius. In contrast, the compact high-harmonic gyrotron operates with a low magnetic field and with Larmor orbits of the beam particles which are comparable to the cavity radius, and which encircle the cavity axis. This may permit the construction of gyrotrons based on permanent magnet technology such as samarium–cobalt.

Typical particle orbits in a conventional gyrotron are shown in Fig. 1(a) and the axis-encircling orbits of the compact high-harmonic gyrotron are shown in Fig. 1(b). The remainder of the introduction consists of a brief description of the current beam production methods with emphasis on their advantages and disadvantages. Finally, the novel system, which is the object of this paper, is discussed.

Most electron guns produce a monoenergetic, unidirectional beam. The obvious way to produce a beam with a large fraction of rotational energy would be to inject the beam at an angle to the background magnetic field [6]. This angle would determine the partition of energy in the beam between the perpendicular and parallel components.

Manuscript received September 22, 1983; revised May 4, 1984. This work was supported in part by U.C.L.A. under Contract 400001, and in part by the U.S. Army Research Office under Contract DAAG29-82-K-0004.

W. H. Miner is with the Fusion Research Center, University of Texas, Austin, TX 78712.
P. Vitello and A. T. Drobot are with Science Applications, Inc., McLean, VA 22102.

0018-9480/84/1000-1293$01.00 ©1984 IEEE

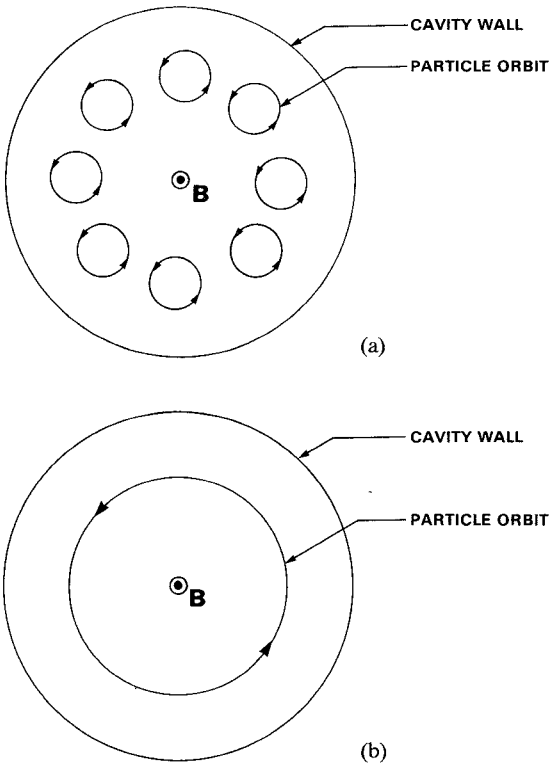

Fig. 1. Schematic diagram of particle orbits in (a) a conventional gyrotron and (b) a high-harmonic gyrotron.

Although this provides a simple way to partition the beam energy, it has an adverse effect on the beam quality. To avoid this problem, the beam could be injected along the magnetic field lines which pass through the resonant cavity and a structure provided to convert the streaming energy into rotational energy. This could be achieved by propagating the electron beam through a variation in the external magnetic field. Magnetic configurations which have been tried include a rippled field [7], a wiggler field [8], and a cusp [9]. As in the case of cross-field injection, the total beam energy is determined by the diode voltage.

The problem of a complex magnetic field structure can be avoided if a more sophisticated electron gun is used. "Magnetron injection"-type electron guns [3], [10], [11] directly produce an electron beam with a velocity component perpendicular to the magnetic field. The ratio of perpendicular energy to parallel energy of the beam produced by this type of gun may be increased by adiabatically compressing the beam, at the expense of increasing the beam thermal spread.

In all the examples previously discussed, the available free energy has been that fraction of the original beam energy acquired in the diode that can be converted to rotational energy. There are also methods for straightforwardly increasing the beam energy by imparting rotational energy to the electron beam. A simple procedure is to pass a cold beam streaming along an external magnetic field through a set of deflection plates analogous to those in a conventional cathode ray tube [12]. An electric field oscillating near the cyclotron frequency applied to the deflection plates will impart rotational energy to the beam. A more efficient method however, and this is the technique to be addressed in this paper, would be to pass the streaming beam through a resonant cavity driven in a TE_{111} mode [13]. In this situation, the phase relation between the beam electrons and the cavity mode is such that the rotational energy of the beam increases at the expense of the cavity radiation fields.

The use of this accelerator cavity to produce a highly energetic helical beam with large pitch ($\alpha = V_\perp / V_\parallel$) has several advantages over the previous methods. The device itself is technically simple. There is no need for a complicated magnetic structure to redistribute the beam energy from streaming to rotational. A much simpler electron gun, such as one of the Pierce type, may be used instead of the more complex magnetron injection gun. The most important advantage of the accelerator cavity is that the amount of rotational energy in the final beam is provided by the cavity and not by the gun. The gun itself is inherently at low voltage and low current. High total beam power is achieved by imparting a large voltage in the accelerator cavity. This produces a low perveance beam avoiding deleterious space charge effects.

The first effort to produce such a spiral beam by passing a linear beam through a resonant cavity was performed by Jory and Trivelpiece [13]. This work contained both an experiment and a numerical study on the interaction of the electron beam with various types of electromagnetic waves: traveling, standing, linear polarization, circular polarization, etc. The experiment demonstrated the production of a spiral beam by passing an axial beam through a resonant cavity driven in a TE_{111} mode. The goal of this paper is to determine the necessary parameters required to produce a relativistic electron beam of a specified rotational energy and pitch (α) for injection into a high-harmonic TE_{m11} gyrotron. The effects of finite beam parameters, thermal spread and radial extent, and cavity power requirements will also be discussed. At the present time, an experiment using a TE_{111} resonant cavity accelerator coupled to a TE_{m11} gyrotron is under way at U.C.L.A., Los Angeles, CA [4].

The model employed for the numerical study is presented in Section II. The particle acceleration mechanism is discussed in Section III. The results of the parametric studies are given in Section IV and the implications derived from these results are discussed in Section V.

II. Physical Model

The experimental device is shown schematically in Fig. 2. An axial, low-voltage electron beam is produced by an electron gun and is propagated down a drift tube guided by a constant background magnetic field B_0, in the z direction. The beam then enters the accelerator cavity, a right cylindrical resonant cavity of length L and radius a which is driven in a circularly polarized TE_{111} mode. The beam interacts with the RF fields of the cavity driven by an external source and then the modulated beam exits the accelerator cavity into a drift tube. The beam propagates down the drift tube until it enters the gyrotron cavity. This work describes the evolution of the beam in the accelerator cavity.

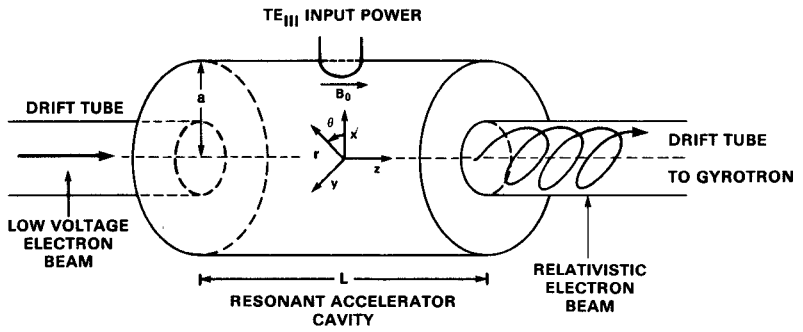

Fig. 2. Schematic diagram of a TE_{111} resonant accelerator cavity.

Using the normalized velocity variable

$$\vec{U} = \gamma \frac{\vec{v}}{c} \tag{1}$$

where the relativistic factor γ is defined by

$$\gamma = \left(1 - \frac{v^2}{c^2}\right)^{-1/2} \tag{2}$$

the equations of motion may be expressed in cylindrical coordinates as

$$\frac{dR}{dt} = \frac{c}{\gamma} U_R \tag{3a}$$

$$\frac{d\theta}{dt} = \frac{c}{R\gamma} U_\theta \tag{3b}$$

$$\frac{dz}{dt} = \frac{c}{\gamma} U_z \tag{3c}$$

$$\frac{dU_R}{dt} = -\frac{|e|}{m_0 c}\left[E_R - \frac{U_z}{\gamma} B_\theta\right] + \frac{U_\theta}{\gamma}\left[\frac{cU_\theta}{R} - \frac{|e|}{m_0 c} B_z\right] \tag{4a}$$

$$\frac{dU_\theta}{dt} = -\frac{|e|}{m_0 c}\left[E_\theta + \frac{U_z}{\gamma} B_R\right] - \frac{U_R}{\gamma}\left[\frac{cU_\theta}{R} - \frac{|e|}{m_0 c} B_z\right] \tag{4b}$$

$$\frac{dU_z}{dt} = -\frac{|e|}{m_0 c}\left[\frac{U_R}{\gamma} B_\theta - \frac{U_\theta}{\gamma} B_R\right]. \tag{4c}$$

In order to simplify the notation, the following normalizations are used:

$$r = R/a \tag{5a}$$

$$\xi = z/L \tag{5b}$$

$$\tau = \frac{c}{a} t \tag{5c}$$

$$\vec{e} = \frac{|e|a}{m_0 c^2} \vec{E} \tag{5d}$$

$$\vec{b} = \frac{|e|a}{m_0 c^2} \vec{B}. \tag{5e}$$

A more useful set of momentum variables for components perpendicular to the background magnetic field are U and Λ where

$$U_R = U \sin(\Lambda) \tag{6a}$$

$$U_\theta = U \cos(\Lambda). \tag{6b}$$

With the normalization given above, (5) may be expressed in terms of the new variables as

$$\frac{dU}{d\tau} = -\left[e_r - \frac{U_\xi}{\gamma} b_\theta\right] \sin(\Lambda) - \left[e_\theta + \frac{U_\xi}{\gamma} b_r\right] \cos(\Lambda) \tag{7a}$$

$$U \frac{d\Lambda}{d\tau} = -\left[e_r - \frac{U_\xi}{\gamma} b_\theta\right] \cos(\Lambda) + \left[e_\theta + \frac{U_\xi}{\gamma} b_r\right] \sin(\Lambda) + \frac{U}{\gamma}\left[\frac{U}{r}\cos(\Lambda) - b_\xi\right] \tag{7b}$$

$$\frac{dU_\xi}{d\tau} = -\frac{U}{\gamma}\left[b_\theta \sin(\Lambda) - b_r \cos(\Lambda)\right]. \tag{7c}$$

The electromagnetic fields inside the resonant cavity are given by the solutions to Maxwell's equations corresponding to TE modes. The solutions are

$$e_\theta = E_0 \frac{\partial J_m(kr)}{\partial(kr)} \sin(m\theta - \omega\tau) \sin(p\xi) \tag{8a}$$

$$b_r = \frac{\delta p}{\omega} E_0 \frac{\partial J_m(kr)}{\partial(kr)} \cos(m\theta - \omega\tau) \cos(p\xi) \tag{8b}$$

$$e_r = -E_0 \frac{mJ_m(kr)}{kr} \cos(m\theta - \omega\tau) \sin(p\xi) \tag{8c}$$

$$b_\theta = -\frac{\delta p}{\omega} E_0 \frac{mJ_m(kr)}{kr} \sin(m\theta - \omega\tau) \cos(p\xi) \tag{8d}$$

$$b_\xi = \frac{k}{\omega} E_0 J_m(kr) \cos(m\theta - \omega\tau) \sin(p\xi) \tag{8e}$$

where $\delta = a/L$, E_0 is the dimensionless RF amplitude, and the normalized cavity frequency is

$$\omega = \left(k^2 + \delta^2 p^2\right)^{1/2} \tag{9}$$

$$p = k_z L \tag{10}$$

$$k_z = l\pi/L \tag{11a}$$

$$k = x_{mn} \tag{11b}$$

where x_{mn} is the nth zero of the first derivative of the mth Bessel function. The final form of the equations of motion are obtained by substituting the expressions for the fields given above, (8), and the background magnetic field into (7), and the results are

$$\frac{dU}{d\tau} = \frac{E_0}{2} \sin(p\xi) \cdot \{J_{m+1}(kr) \sin(m\theta - \omega\tau + \Lambda) - J_{m-1}(kr) \sin(m\theta - \omega\tau - \Lambda)\} + \frac{\delta p U_\xi}{\omega} \frac{E_0}{2} \cos(p\xi) \cdot \{J_{m+1}(kr) \cos(m\theta - \omega\tau + \Lambda) - J_{m-1}(kr) \cos(m\theta - \omega\tau - \Lambda)\} \tag{12a}$$

$$U\frac{d\Lambda}{d\tau} = \frac{E_0}{2}\sin(p\xi)\cdot\{J_{m+1}(kr)\cos(m\theta-\omega\tau+\Lambda) + J_{m-1}(kr)\cos(m\theta-\omega\tau-\Lambda)\} - \frac{\delta pU_\xi}{\gamma\omega}\frac{E_0}{2}\cos(p\xi)\cdot\{J_{m+1}(kr)\sin(m\theta-\omega\tau+\Lambda) + J_{m-1}(kr)\sin(m\theta-\omega\tau-\Lambda)\} + \frac{U}{\gamma}\left\{\frac{U}{r}\cos(\Lambda)-b_0-\frac{k}{\omega}E_0J_m(kr)\cdot\cos(m\theta-\omega\tau)\sin(p\xi)\right\} \quad (12b)$$

$$\frac{dU_\xi}{d\tau} = -\frac{\delta pU}{\gamma\omega}\frac{E_0}{2}\cos(p\xi)\cdot\{J_{m+1}(kr)\cos(m\theta-\omega\tau+\Lambda) - J_{m-1}(kr)\cos(m\theta-\omega\tau-\Lambda)\}. \quad (12c)$$

A test particle approach is taken to describe the dynamic evolution of the electron beam. In this approach, the dynamics of individual particles are calculated and the properties of the beam are determined by averaging over the beam particle distribution function.

The individual particle dynamics are obtained by numerically integrating the equations of motion. A fourth-order Adams–Moulton predictor–corrector scheme is used to advance the equations in time. The particle dynamics are followed until the particles exit the cavity through either aperture or intersect the cavity wall.

In order to determine the dominant physical processes involved in the beam dynamics, the physical model has been somewhat simplified. The first simplifying assumption is that the self-fields of the beam are neglected with respect to the wave fields of the cavity modes. Secondly, the exact fields for a closed right circular resonant cavity are used and the effects of finite apertures for the entrance and exit of the beam and microwave input are neglected.

III. Accelerating Mechanism

For a beam injected on axis into a resonant cavity driven in a circularly polarized TE_{111} mode, the particles see, to lowest order, a circularly polarized monochromatic plane standing wave. If the difference between the wave frequency and the cyclotron frequency is sufficiently small, i.e.,

$$\left|\omega \pm \frac{\delta pU_\xi}{\gamma} - \frac{b_0}{\gamma}\right| \ll \omega \quad (13)$$

the particles become synchronized with the wave and gain energy. This effect was first recognized by Davydovskii [14].

Since the beam is injected on axis, the equations of motion may be simplified by expanding the Bessel function terms about the origin. Keeping only the lowest order expansion term, the equations of motion are approximated by

$$\frac{dU}{d\tau} = -\frac{E_0}{2}\left[\sin\psi\sin(p\xi)+\frac{\delta pU_\xi}{\gamma\omega}\cos\psi\cos(p\xi)\right] \quad (14a)$$

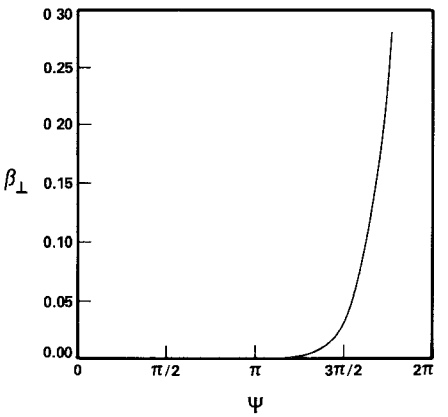

Fig. 3. Early time evolution of the wave-particle phase.

$$U\frac{d\psi}{d\tau} = \frac{-E_0}{2}\left[\cos\psi\sin(p\xi)+\frac{\delta pU_\xi}{\gamma\omega}\sin\psi\cos(p\xi)\right] - U\left(\omega-\frac{b_0}{\gamma}\right) \quad (14b)$$

$$\frac{dU_\xi}{d\tau} = \frac{E_0}{2}\frac{\delta pU}{\gamma\omega}\cos\psi\cos(p\xi) \quad (14c)$$

where

$$\psi \equiv \theta - \omega\tau - \Lambda. \quad (15)$$

The fact that the beam particles gain energy can easily be seen by combining (14a) and (14c) to yield

$$\frac{d}{d\tau}\left(U^2+U_\xi^2\right) = -UE_0\sin(\psi)\sin(p\xi). \quad (16)$$

Since, for the TE_{111} mode, $\sin(p\xi) > 0$ there will be a positive change in the energy provided

$$\pi \leqslant \psi \leqslant 2\pi \quad (17)$$

with the maximum gain occurring when

$$\psi = \frac{3\pi}{2}. \quad (18)$$

When the cavity is driven with $\delta pU_\xi/\gamma\omega \ll 1$ (as is the case for the present study) and $\omega - b_0/\gamma \ll \omega$, (14b) shows that ψ will in fact always evolve to $3\pi/2$. The early time behavior of the perpendicular velocity $\beta_\perp$ versus ψ is shown in Fig. 3.

After a sufficient period of growth, the beam relativistic factor γ becomes large enough to violate the synchronism condition, (13), and the particles begin to slip in phase relative to the wave. As the particles slip in phase, the rate of gain decreases until the criteria given in (17) are no longer satisfied and they begin to lose energy.

To lowest order, neglecting the RF field, the solutions to the equations of motion are all constants corresponding to a drifting beam with no transverse velocity

$$U^{(0)} = 0 \quad (19a)$$

$$\psi^{(0)} = \frac{3\pi}{2} \quad (19b)$$

$$U_\xi^{(0)} = \overline{U}_\xi \quad (19c)$$

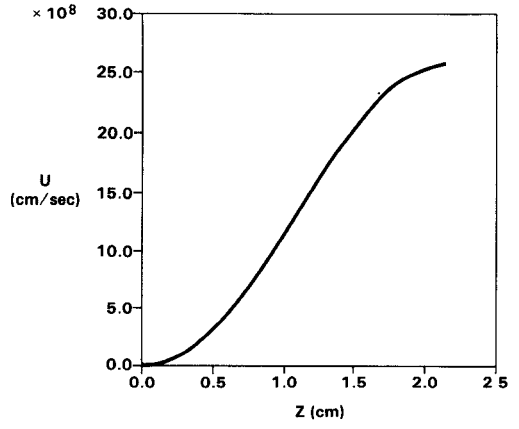

(a)

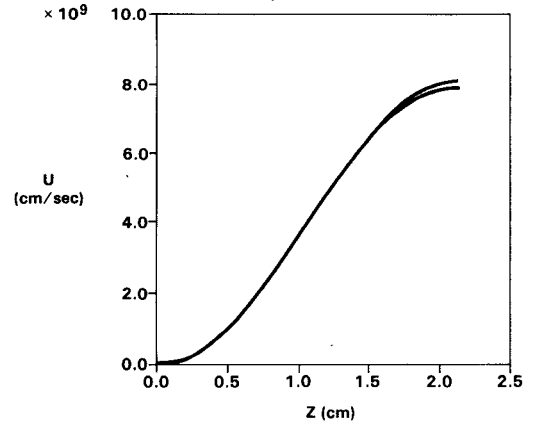

(b)

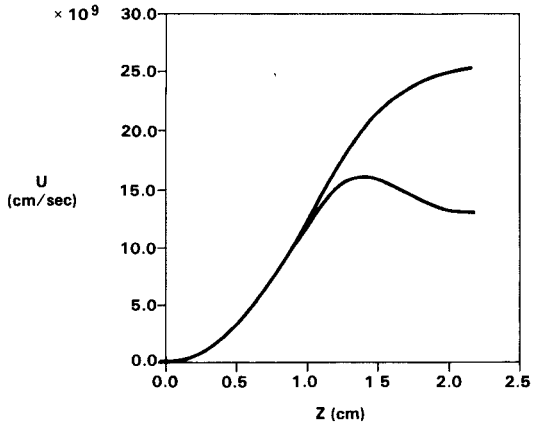

(c)

Fig. 4. Comparison between analytical and numerical calculations of the perpendicular velocity for three values of the parameter E_0: (a) $E_0 = 0.010$, (b) $E_0 = 0.032$, (c) $E_0 = 0.100$.

where $\overline{U}_\xi$ is determined by the initial beam energy by

$$\overline{U}_\xi = \left(\gamma_i^2 - 1\right)^{1/2}. \tag{20}$$

The first-order solution for the perpendicular momentum is

$$U^{(1)} = \frac{E_0 \gamma_i}{\delta p \overline{U}_\xi} \sin^2\left(\frac{\delta p \overline{U}_\xi \tau}{2\gamma_i}\right). \tag{21}$$

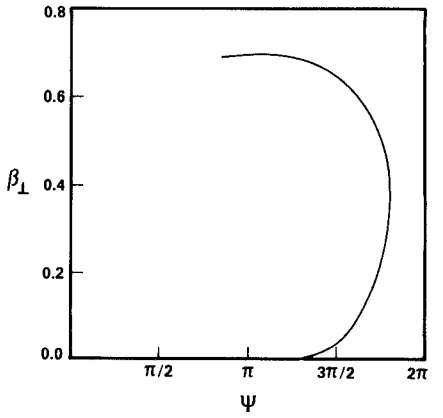

Fig. 5. Evolution of the wave-particle phase as the beam passes through the accelerator cavity.

Comparison between the analytic result and the numerical code as a function of the perturbation parameter E_0 is shown in Fig. 4(a)–(c) for a cavity with $a = 1.3$ cm, $L = 2.16$ cm, and an initial beam of 1 keV. In Fig. 4(a), the difference between the analytical result and the numerical result cannot be distinguished. In Fig. 4(b), the solutions begin to diverge near $z \sim 1.6$ cm as the beam has gained enough energy to violate the synchronism condition, (13). Finally in Fig. 3(c), E_0 is so large as to cause a violation of the synchronism condition at $z \sim 1.0$ cm and the linear theory is no longer valid.

IV. Numerical Simulation Results

The efficiency of the gyroresonant acceleration depends critically on three parameters: 1) b_0, the background magnetic field which determines the phase relation between the cavity mode and the cyclotron frequency, i.e., $\omega - b_0/\gamma$; 2) E_0, the RF amplitude of the cavity mode; and 3) γ_i, the initial energy of the input beam. The effects of variations in all of these critical parameters will be discussed in this section. We use a cavity as before with $a = 1.3$ cm, $L = 2.16$ cm, and an initial beam energy of 1 keV. The beam is injected with zero transverse velocity.

The temporal evolution of the beam as it passes through the acceleration cavity is determined by numerically integrating the systems of (3) and (4). Particle trajectories are begun at the entrance aperture and end either when the particle leaves the cavity through the exit aperture or intersects the cavity wall. The beam evolution is also stopped if the particle is reflected and leaves the cavity through the entrance aperture. The effects of entrance and exit apertures are neglected, as are the self-fields of the beam.

The long timescale evolution of the perpendicular velocity is shown in Fig. 5. The beam gains perpendicular velocity rapidly, but when it reaches $\beta_\perp \sim 0.4$ it begins to slip backward in phase. The particles have gained so much energy that γ has increased sufficiently to violate the synchronism condition, (13). The particles continue to gain energy, but at a lower rate, and continue to slip in the wave phase. Finally, the beam reaches a position where (17) is violated and the beam begins to lose energy.

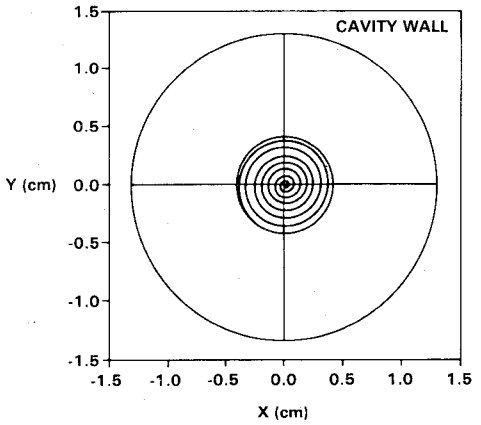

Fig. 6. Trajectory of a typical beam projected onto the $x-y$ plane as it passes through the accelerator cavity.

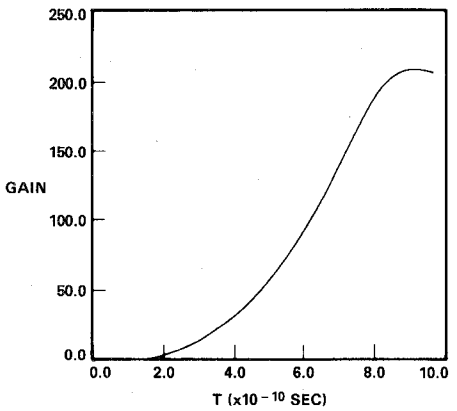

Fig. 7. Gain in energy of the electron beam as a function of time as it passes through the accelerator cavity.

More details of the beam evolution are given in Figs. 6 and 7. The spatial trajectory of the beam in the cross section of accelerator cavity is shown in Fig. 6. The beam enters the cavity and follows a spiral trajectory, exiting the cavity with a radius of approximately 0.4 cm. Since the beam is no longer gaining rotational energy as it exits the cavity, the radius thereafter remains constant. The gain in beam energy as a function of its position along the axis of the accelerator cavity is shown in Fig. 7. The gain is defined by

$$G = \frac{\gamma_f - \gamma_i}{\gamma_i - 1} \tag{22}$$

where the subscripts i and f refer to initial and final, respectively. This is the ratio of the change in the kinetic energy of the beam to its initial kinetic energy.

The goal of this work is to demonstrate that a beam suitable for injection into a gyrotron can be produced in an accelerator cavity. To this end, a parametric study was performed varying the constant background magnetic field and the RF amplitude in the accelerator cavity. The studies were done by choosing an RF amplitude and varying the background magnetic field through the resonance

$$\omega - \frac{b_0}{\gamma_i} = 0 \tag{23}$$

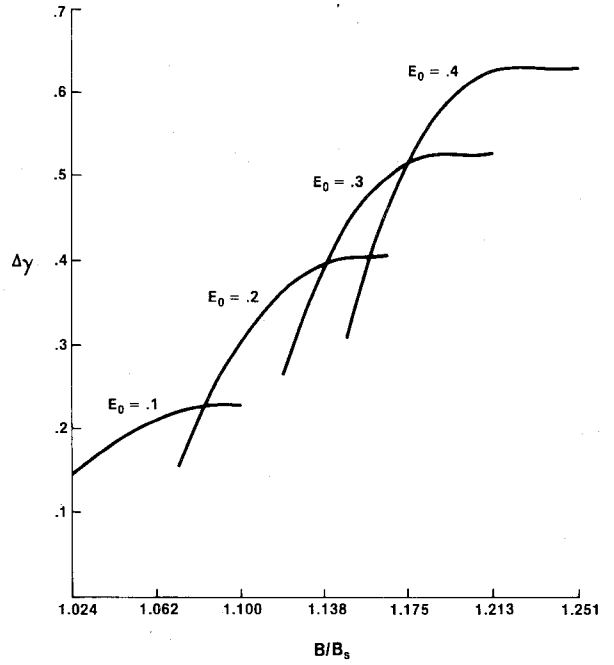

Fig. 8. Change in energy of the electron beam as a function of the background magnetic field for four values of the RF amplitude in the accelerator cavity.

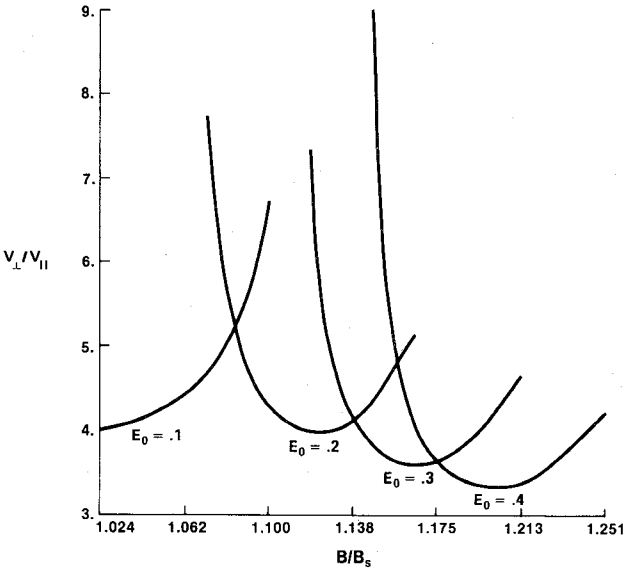

Fig. 9. Final value of the pitch of the beam trajectory as it exits the cavity as a function of the background magnetic field for four values of the RF amplitude in the accelerator cavity.

and observing the beam characteristics as it exits the cavity. The characteristics of interest which were discussed in the introduction are the change in beam energy $\Delta\gamma = \gamma_f - \gamma_i$ and the pitch of the beam α. The results of the studies are shown in Figs. 8 and 9. The magnetic field in these figures is normalized to the synchronous value of the field for a particle at rest, i.e.,

$$B_s = \frac{m_0 c \omega}{|e|}. \tag{24}$$

Fig. 8 shows that large changes in the beam energy may be

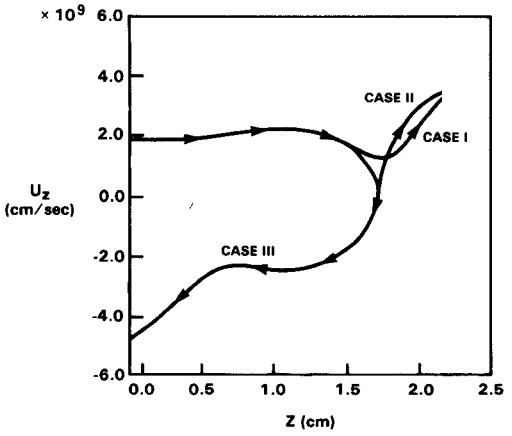

Fig. 10. Plot U_z versus z for three values of the background magnetic field in the neighborhood of a "cutoff."

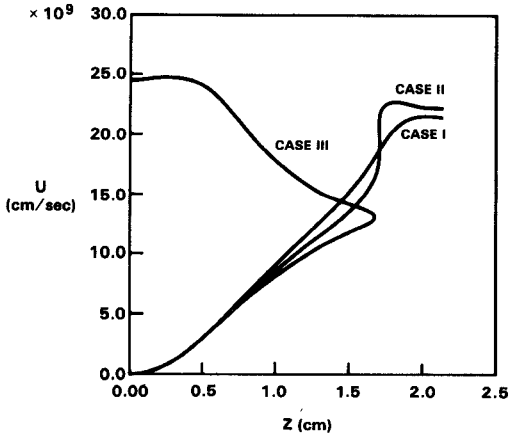

Fig. 11. Plot of U versus z for three values of the background magnetic field in the neighborhood of a "cutoff."

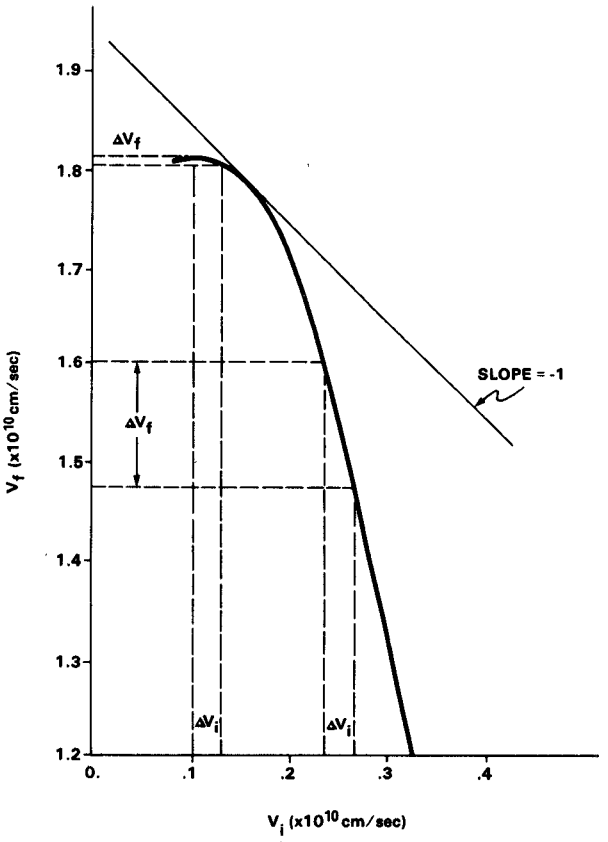

Fig. 12. Final beam velocity as a function of input beam velocity showing regions where beam quality is enhanced and regions when beam quality is degraded.

obtained in the accelerator cavity but that they are obtained in a narrow range of magnetic field. This requires accurate tuning of the magnetic field for a given RF amplitude and wave frequency. The "cutoff" at either end of these curves occurs because the beam is reflected in the cavity and therefore does not reach the exit aperture. For fixed E_0, there may actually be more than one region of magnetic field for which the beam can pass through the cavity. These other regions were found to have much smaller values of G, and were therefore not investigated.

In order to demonstrate the physics of the "cutoff" of the beam (see Fig. 8), three cases with different values of B/B_s in the vicinity of the upper "cutoff" are compared. The first two of these cases correspond to points on the curve labeled $E_0 = 0.1$, for values of B/B_s of 1.0905 and 1.100 in Fig. 8, and the third case corresponds to the same value of E_0 but for B/B_s 1.1095. Figs. 10 and 11 are plots of U_z versus z and U versus z for these cases.

At early times, U_z remains nearly constant since the only force acting in the z direction is

$$F_z = -|e|\frac{\vec{U}}{\gamma} \times \vec{B} \tag{25}$$

($E_z \equiv 0$ for TE modes) and initially $U \equiv 0$. As the beam spins up, U increases, and the Lorentz force in the z direction begins to modulate the beam velocity along the axis. Since $U_\theta \gg U_r$, the force along the axis is determined by the radial magnetic field. Fig. 10 shows that, for case I, the beam passed through three phases of the field which alternated between accelerating and decelerating the beam along the axis. For case II, the axial motion of the beam was nearly stopped during the decelerating phase as U_z approached zero. Finally, for case III, the beam was reflected, U_z became negative, and the beam left the cavity through the entrance aperture. Such beam cutoffs have been observed experimentally [15]. Similar numerical results were obtained by Jory and Trivelpiece [13].

Maximum gain occurs at the high field "cutoff" just before the beam is reflected. This allows the beam to interact with the cavity RF fields for the maximum length of time. This effect is also demonstrated in Fig. 12. Fig. 12 shows the final beam velocity as a function of the initial beam velocity for fixed values of $E_0 = 1$ and $b_0 = 2.9$. For large values of the initial velocity, the beam passes through the cavity too quickly to interact with the RF fields. As the initial velocity decreases, the interaction time increases and the beam begins to gain energy. Finally, when the initial velocity becomes too small, the beam is reflected.

The effects of a velocity distribution of particles in the input beam can also be determined from Fig. 12. The space of initial velocities can be divided into two regions by observing where a tangent line of slope $= -1$ intersects the curve in Fig. 12. Thermal beams whose drift velocities are

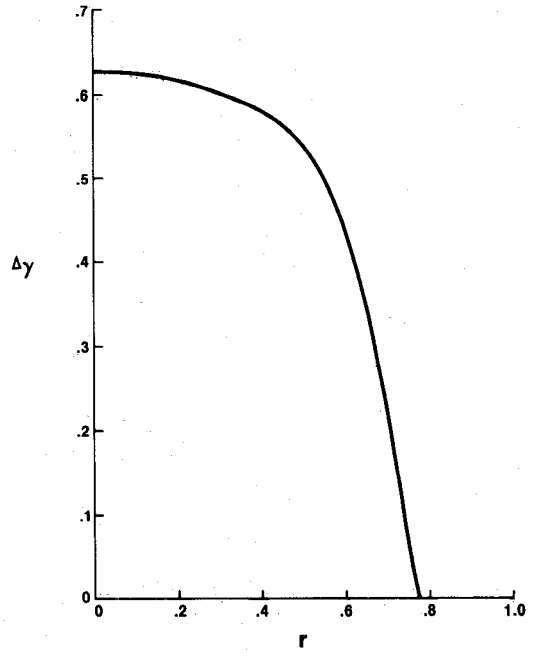

Fig. 13. Change in energy as a function of the initial radial position of the beam.

greater than this critical velocity will have their thermal spread enhanced, while similar beams whose drift velocities are less will have their thermal spread reduced. Optimal experimental conditions, i.e., maximum gain, would therefore in general produce an output beam which has less thermal spread than the input beam.

In addition to variations in velocity space, the effects of variation in physical space were also considered. The effect of a finite radial extent of the beam was determined by moving the injection point off-axis and observing the resulting effect on the change in energy of the beam. The results are presented in Fig. 13. Fig. 13 shows that for injection out to a radius of one-half the cavity radius the gain in energy decreases only about 15 percent. However, beyond this point the beam sees relatively weak fields and the gain drops drastically. Therefore, for beams whose radius is less than half the cavity radius, the radial extent should have a negligible effect upon the energy gained.

In order to determine the overall efficiency of the cyclotron resonant accelerator, it is necessary to determine what fraction of the input power can actually be transferred to the electron beam. The input power can be expressed by

$$P_{\mathrm{IN}} = \frac{\omega W}{Q_L} + IV_b \tag{26}$$

where ω is the frequency, W is the stored energy, Q_L is the loaded cavity quality factor, I is the beam current, and V_b is the beam voltage gained in the cavity, i.e., $V_b = V_f - V_i$ where V_i is the initial beam voltage, gained in the diode, and V_f is the final beam voltage as it exits the accelerator cavity. The first term on the right-hand side of (26) accounts for resistive and diffractive losses in the cavity and the second term represents energy transferred to the electron beam.

For a circularly polarized mode in a right circular resonant cavity, the energy stored in the cavity is

$$W = \frac{E_0^2 La^2}{16}\left(\frac{m_0c^2}{|e|}\right)^2\left[\left(1-\left(\frac{m}{ka}\right)^2\right)J_m^2(ka)\right]. \tag{27}$$

If the cavity is driven at a frequency ω and the loaded quality factor of the cavity is known, then the cavity loss term may be calculated as a function of the RF amplitude parameter E_0.

The power transferred to the beam as it passes through the cavity is

$$\delta P_b = I(\gamma_f - \gamma_i)\frac{m_0c^2}{|e|} = I\Delta\gamma\frac{m_0c^2}{|e|}. \tag{28}$$

An optimal value of $\Delta\gamma$ for a given value of the RF amplitude parameter E_0 is used (see Fig. 8). With this one-to-one correspondence between $\Delta\gamma$ and E_0, it is possible to generate a set of curves showing what fraction of the input power goes into the electron beam as a function of the input power, parameterized by $\Delta\gamma$ and I. These curves are shown in Fig. 14. The curves are extremely useful in

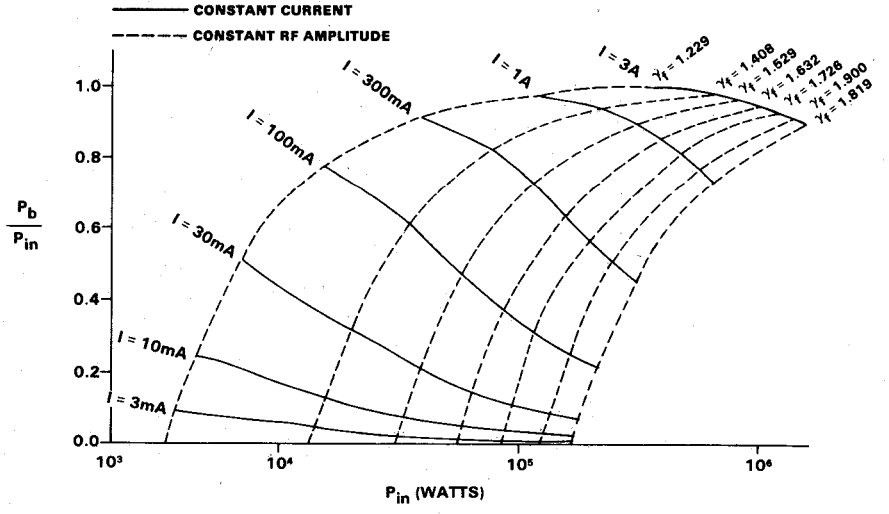

Fig. 14. Fraction of the input power going into the beam as a function of the input power.

that they prescribe the experimental requirements for obtaining an output beam of a specific voltage as a function of both input power and beam current.

V. Discussion

We have studied the optimum operating parameters at which the TE_{111} accelerator cavity will produce a spiral relativistic electron beam. It has been shown that, operating under these conditions, it is possible to obtain beam energies and pitch in the range $1.1 \lesssim \gamma_f \lesssim 1.6$ and $3.0 \lesssim \alpha \lesssim 9.0$ for cavity RF amplitudes in the range $0.1 \leqslant E_0 \leqslant 0.4$. A set of power curves has been generated which can be used to determine appropriate operating regimes which are parameterized by input power level, beam current, and the desired value of γ_f. Higher values of γ_f are obtainable for even larger E_0.

The effects of variations in both velocity space and in physical space were determined. It was shown that it is possible to improve the quality of the beam from the gun in the accelerator cavity under appropriate conditions and that the radial extent of the beam will have a negligible effect if the beam radius is less than half the cavity radius.

Work remains to be done in more accurately modeling the accelerator by including field leakage through the apertures and the self-field of the beam. Methods for improving the accelerator performance through cavity tapering and varying the background magnetic field are also under consideration.

References

[1] V. A. Flyagin, A. V. Gaponov, M. I. Petelin, and V. K. Yulpatov, "The gyrotron," *IEEE Trans. Microwave Theory Tech.*, vol. MTT-25, pp. 514–521, 1977.

[2] J. L. Hirshfield and V. L. Granatstein, "The electron cyclotron maser—An historical survey," *IEEE Trans. Microwave Theory Tech.*, vol. MTT-25, pp. 522–527, 1977.

[3] A. V. Gaponov, V. A. Flyagin, A. L. Gol'denberg, G. S. Nusinovich, Sh. E. Tsimring, V. G. Usov, and S. N. Vlasov, "Powerful millimetre-wave gyrotrons," *Int. J. Electron.*, vol. 51, pp. 277–302, 1981.

[4] D. B. McDermott, N. C. Luhmann, Jr., and A. Kupiszewski, "Small-signal theory of a large-orbit electron-cyclotron harmonic maser," *Phys. Fluids*, vol. 26, pp. 1936–1941, 1983.

[5] P. Vitello, W. G. Miner, and A. T. Drobot, "Theory and numerical modeling of a compact low-field high frequency gyrotron," *IEEE Trans. Microwave Theory Tech.*, vol. MTT-32, pp. 373–386, Apr. 1984.

[6] S. Ono, K. Yamanouchi, Y. Shibata, and Y. Koike, "Cyclotron fast-wave tube using spatial harmonic interaction—The traveling wave peniotron," in *Proc. 4th Int. Congress of Microwave Tubes* (Schevinginger), 1962, p. 353.

[7] V. L. Granatstein, M. Herndon, P. Sprangle, Y. Carmel, and J. A. Nation, "Gigawatt microwave emission from an intense relativistic beam," *Plasma Phys.*, vol. 17, pp. 23–28, 1975.

[8] J. L. Hirshfield, I. B. Bernstein, and J. M. Wachtel, "Cyclotron resonance interaction of microwaves with energetic electrons," *IEEE J. Quantum Electron.*, vol. QE-1, pp. 237–245, 1965.

[9] C. Kyler and K. R. Chu, "Generation and improvement of the gyrotron electron beam in a biased cusp magnetic field," NRL Memo, Rep. 4401, 1981.

[10] J. L. Seftor, A. T. Drobot, and K. R. Chu, "An investigation of a magnetron gun suitable for use in a cyclotron maser," *IEEE Trans. Electron Devices*, vol. ED-26, pp. 1609–1616, 1979.

[11] A. W. Fliflet, A. J. Dudas, M. E. Read, and J. M. Baird, "Use of electrode synthesis technique to design MIG-type guns for high power gyrotrons," *Int. J. Electron.*, vol. 53, pp. 743–755, 1982.

[12] T. Wessel-Berg, in *Proc. 6th Int. Conf. on Infrared and Millimeter Waves* (Miami, FL), 1982.

[13] H. R. Jory and A. W. Trivelpiece, "Charged-particle motion in large-amplitude electromagnetic fields," *J. Appl. Phys.*, vol. 39, pp. 3053–3060, 1968.

[14] V. Y. Davydovskii, "The possibility of accelerating charged particles by electromagnetic waves in a constant magnetic field," *Sov. Phys. JETP*, vol. 16, p. 629, 1963.

[15] D. B. McDermott, private communication, 1983.

[16] A. Kupiszewski, Masters thesis, U.C.L.A., Los Angeles, CA, 1982.

William H. Miner, Jr., was born in Jacksonville, NC, on August 27, 1949. He received the B.A. degree in physics from Rollins College, Winter Park, FL, in 1971 and the Ph.D. degree in physics from the University of Texas, Austin, in 1978.

He was currently a member of the Technological Systems Group at Science Applications, Inc., McLean, VA, where he was involved in analytical and numerical investigations of microwave generation and diode physics. In the area of microwave generation, he studied the physics of compact, high-harmonic gyrotrons. He also investigated the stability of electron flow in planar diodes. He is currently with the Fusion Research Center, University of Texas at Austin, where he is studying transport phenomena in tokamak plasmas.

Dr. Miner is a member of the American Physical Society.

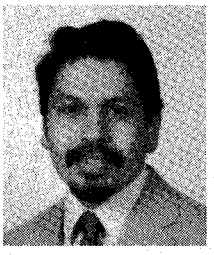

Peter Vitello was born in Glendale, CA, on September 15, 1950. He received the B.S. degree in physics in 1972 from the University of Southern California, Los Angeles, and the Ph.D. degree in theoretical physics in 1977 from Cornell University, Ithaca, NY.

He is a member of the Plasma Physics Division at Science Applications, Inc., McLean, VA. He is currently working on high-harmonic gyrotron oscillators and gyro-klystron amplifiers.

Dr. Vitello is a member of the American Physical Society and of the American Astronomical Society.

Adam T. Drobot was born in Zakopane, Poland, on May 13, 1947. He received the B.S. degree in engineering physics from Cornell University, Ithaca, NY, in 1968 and the Ph.D. degree in physics from the University of Texas, Austin, in 1974.

He has been working at Science Applications, Inc., McLean, VA, on the application of numerical and computational techniques to the simulation of complex physical systems involving the interaction of electromagnetic fields with high-density energetic particles. He has contributed recently to work on collective ion acceleration, free-electron lasers, the basic theory and simulation of high-power microwave sources such as gyrotrons, magnetrons, and klystrons. He is currently involved in problems of power flow in high-power magnetically insulated transmission lines and in intense relativistic diodes.

Dr. Drobot is the manager of the Plasma Physics Division in the Technological Systems Group at Science Applications, Inc. He is a member of the American Physical Society, Sigma Phi Sigma, and Phi Kappa Phi.